Available online at www.sciencedirect.com
ScienceDirect
Ceramics International 34 (2008) 311–316
CERAMICS INTERNATIONAL
www.elsevier.com/locate/ceramint

Self-reinforced Ca-hexaluminate/alumina composites with graded microstructures

D. Asmi [a], I.M. Low [b,*]

[a] Department of Physics, Faculty of Mathematics and Natural Sciences, Lampung University Jl. S. Brojonegoro, No. 1 Bandar, Lampung 35145, Indonesia
[b] Materials Research Group, Department of Applied Physics, Curtin University of Technology, GPO Box U 1987, Perth, WA, Australia

Received 24 July 2006; received in revised form 9 September 2006; accepted 4 October 2006
Available online 18 December 2006

Abstract

The physical, thermal, and mechanical characteristics of self-reinforced calcium-hexaluminate/alumina composites with a graded microstructure are described. The presence of CA_6 phase in Al_2O_3 matrix has a significant effect on the physical, thermal, and mechanical properties of graded Al_2O_3–CA_6 composites. The slightly lower shrinkage and density in the graded composite can be attributed to the presence of CA_6 phase. The thermal expansion and densification behaviour of the graded composite showed that the presence of CA_6 phase hinders the processes of sintering and densification of alumina matrix. When compared to the alumina region, the graded CA_6–Al_2O_3 region is softer by virtue of the presence of the softer CA_6 phase. However, the fracture toughness in the graded region is higher than the alumina region which can be attributed to the display of crack deflection and crack-bridging provided by the CA_6 platelets.

Keywords: B. Composites; B. Platelets; C. Fracture; C. Mechanical properties; D. Al_2O_3

1. Introduction

Alumina (Al_2O_3) is the most commonly used ceramic oxide industrial material due to its superior hardness, corrosion resistance, oxidation resistance, and chemical stability. However, the application of alumina as a structural ceramic is limited due to its relatively low fracture toughness and thermal-shock resistance. In order to improve the mechanical properties, whiskers, fibres, or platelets may be dispersed within the alumina matrix due to their enhancement of crack defection and grain bridging mechanisms [1–3]. These mechanisms dissipate considerable strain energy through frictional motion of the reinforcement phase against the matrix during elastic stretching, debonding, and pull-out. Thus, increases in the number, diameter, and debond length of such bridging reinforcements would be expected to enhance the toughening effects. However, incorporation of high aspect ratio particles by powder processing results in the formation of transient stresses during sintering, leading to poor densification of the ceramic [4]. Therefore, advanced manufacturing techniques such as colloidal processing, hot pressing, or isostatic pressing are required in order to produce composites with high relative density and good mechanical properties [5–7].

In view of this, interest is growing in the design of toughened ceramics whose microstructures exhibit plate-like grain morphologies. The presence of in situ platelets may act as effective bridging sites in the crack wake, resulting in improved fracture resistance. This concept of ''in situ toughening'' or ''self-reinforcement'' has already been demonstrated for silicon nitride (Si_3N_4) [8–10], silicon carbide (SiC) [11,12], and more recently alumina [13–18] ceramics, where elongated grains are grown within the matrix in order to improve the fracture toughness and Weibull modulus. In self-reinforced silicon nitride ceramics, the controlled nucleation of elongated β-Si_3N_4 grains within the α-Si_3N_4 matrix may result in strength values >1 GPa and toughness values >10.0 MPa $m^{1/2}$. Similar improvements in mechanical properties have also been obtained for self-reinforced SiC through the β → α phase transformation. Using a similar approach, self-reinforced alumina ceramics with improved fracture toughness have been developed through the addition of: CaO to form elongated calcium hexaluminate (CA_6) grains [19,20]. In recent years, Al_2O_3–CA_6 composites have

* Corresponding author. Tel.: +61 8 9266 7544; fax: +61 8 9266 2377.
E-mail address: j.low@curtin.edu.au (I.M. Low).

0272-8842/$34.00.
doi:10.1016/j.ceramint.2006.10.001

been widely studied as structural materials since it was found that Al_2O_3 containing CA_6 *platelets* showed a more pronounced R-curve behaviour than a composite containing equiaxed grains [21–23] It has been shown that the increase in aspect ratio of CA_6 grains increases the crack growth resistance, and the crack morphology is planar when CA_6 grains are equiaxed, and tortuous when they are plates.

Recently, liquid infiltration has emerged as an extremely useful method for tailoring or designs functionally graded ceramic materials. Using this infiltration process, it is possible to design new materials with unique microstructures (i.e. graded, multiphase, microporous, etc.) and unique thermo-mechanical properties (i.e. graded function, designed residual strains, thermal shock, etc.). This technique has been successfully adopted by various researchers to fabricate novel graded materials such as mullite/alumina [24,25], mullite/zirconia-toughened alumina [26], alumina titanate/zirconia-alumina [27,28], and aluminium-titanate/alumina [29,30].

In this paper, we describe the synthesis of a graded and self-reinforced alumina/CA_6 system using an infiltration process. The resultant microstructure has a heterogeneous CA_6/alumina graded layer for toughness and crack dispersion, and a homogeneous alumina layer for hardness and wear resistance. The influence of a graded CA_6 dispersion on the physical, thermal and mechanical properties is discussed.

2. Experimental procedure

The alumina perform was fabricated by uniaxial pressing of alumina powder at 75 MPa to yield samples of dimensions 5 mm × 12 mm × 60 mm. Infiltration of the porous preform was conducted at room temperature by partial immersion in a solution of calcium acetate for 5 h. The infiltrated preform was then dried at room temperature for 24 h prior to heat-treatment in a high temperature furnace at 1400 °C for 12 h to allow for the growth of CA_6 platelets, followed by densification at 1650 °C for 2 h, and then furnace-cooled. Fig. 1 shows a typical microstructure showing the graded distribution of CA_6 platelets in the infiltrated and sintered sample.

The values of bulk density, apparent porosity, and shrinkage of the sintered samples were determined using the Archimedes principle according to Australian Standard [31] with de-ionised water as the immersion medium. The volumetric shrinkage of the samples was determined by measuring their volume before infiltration (V_i) and after sintering (V_f). The volume shrinkage (S_v) was calculated using following equation:

$$S_v = \frac{V_i - V_f}{V_i} \quad (1)$$

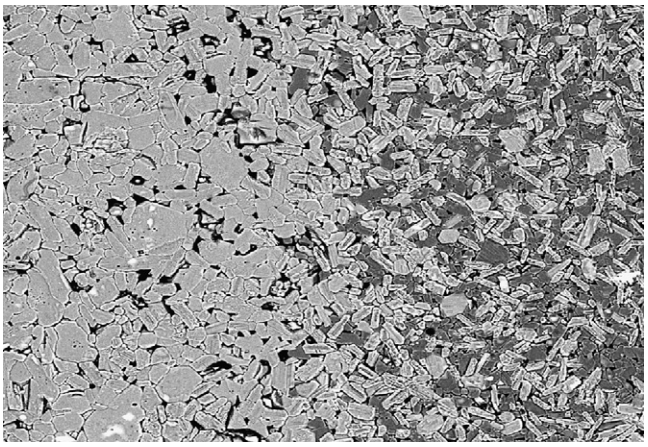

Fig. 1. Back-scattered electron micrograph showing a typical microstructure of an infiltrated and sintered sample showing the graded distribution of CA_6 platelets in the graded region.

The thermal expansion and densification behaviour of green alumina and graded alumina/CA_6 samples at temperature in the range 20–1500 °C using a THETA 160 dilatometer calibrated with a NIST single crystal shappire standard. A bar shaped sample with dimensions of 4 mm × 4 mm × 10 mm was prepared for the measurement. Simultaneous DTA and TGA measurements on the composites were carried out on a Netzsch STA-409C instrument in nitrogen atmosphere.

Indentation hardness was measured using a ZWICK microhardness tester with Vickers diamond pyramid. All the samples used for indentation tests were prepared by cold-mounting in resin and diamond polishing the test surface beginning at 40, 15, 9, 6, 3 μm, and finishing with 1 μm grade diamond. The samples were indented using a load of 98 N with a minimum of three indents made for each measurement. The indentation half-diagonal lengths and the radial surface crack lengths were measured directly using a micrometer attached to the sample stage. The average half-diagonal length and average radial surface crack length were used to calculate hardness and fracture toughness.

3. Results and discussion

3.1. Physical and thermal properties

Table 1 shows the comparative values in shrinkage, density, porosity, and mass change due to infiltration after sintering for both alumina as control and the graded alumina/CA_6. The weight gain measurement method of Criado et al. [32] was used to estimate the amount of CA_6 incorporated into the alumina

Table 1
Values of weight gain, density, porosity, and shrinkage for alumina and graded alumina/CA_6 samples

Sample	Δm (%)	Density (ρ) (g/cm^3)	Porosity (P) (%)	Shrinkage (S_v) (%)
Alumina (control)	−0.8 (2)	3.92 (3)	1.7 (2)	45.3 (2)
Graded alumina/CA_6	8.7 (4)	3.86 (4)	3.6 (3)	38.2 (2)

Δm, weight difference before infiltration and after sintering. Values in parentheses are the estimated standard deviation of the values to the left.

preform. This method is based on the weight difference between the alumina preform prior to infiltration and the composite body after sintering. Note that the CA_6 content calculated using this method yielded a bulk concentration and therefore provided no information on the distribution of the CA_6 within the composite body. As expected, the infiltrated sample increased in mass after sintering with a mass gain of 8.7%. This implies that a new phase had been introduced into alumina preform, i.e. the formation of CA_6 via in situ reaction of alumina and CaO (from decomposition of calcium acetate) as follows:

$$6Al_2O_3 + CaO \rightarrow CaAl_{12}O_{19} \quad (CA_6) \tag{2}$$

Crystallographic density values of 3.786 g/cm^3 for CA_6 (PDF No. 84-1613, ICDD data base) and 3.986 g/cm^3 for α-Al_2O_3 (PDF No. 43-1484) were used to compute the theoretical density for the graded alumina/CA_6 sample based on the rule of mixtures and a value of 3.97 g/cm^3 was obtained. The measured densities for the sintered graded and control samples were 3.86 ± 0.04 and 3.92 ± 0.03 g/cm^3, which represent 97.5 and 98.3% theoretical densities. This suggests that both samples sintered well and achieved near full density. The slightly lower value for the graded sample when compared to the control sample can be attributed to the presence of CA_6 phase, which may hinder the densification process. The porosity results show that the graded sample was slightly more porous than the control sample.

The volume shrinkages of graded and control samples were reduced by as much as 38.2 and 45.3%, respectively, after sintering at 1650 °C for 2 h. The lower shrinkage in the former can be attributed to the formation of CA_6 with a concomitant volume expansion [33].

3.2. Thermal expansion and shrinkage behaviour

Fig. 2 shows the plots of thermal expansion and densification versus temperature for both alumina and graded alumina/CA_6 samples. The starting temperature at both samples commenced to densify was ~1137 °C for alumina and ~1206 °C for the graded sample. The maximum shrinkage of the graded sample occurred at ~1352 °C which is slightly higher than of alumina at ~1347 °C. This implies that the formation CA_6 has hindered the processes of sintering and densification in the graded sample. The average thermal expansion coefficient for the graded sample was 9.11×10^{-6} °C^{-1} which is higher than that of alumina (i.e. 8.63×10^{-6} °C^{-1}).

3.3. Differential thermal and gravimetric analyses (DTA and TGA)

Fig. 3 shows the simultaneous DTA and TGA plots for the calcium acetate as recorded in the temperature range 20–1500 °C. A heating rate of 10 °C/min was used to carry out this analysis. Two small endothermic peaks at 162 and 206 °C in the DTA curve (Fig. 3a) associated with the first weight lost in the TGA curve (Fig. 3b) can be attributed to a two-step dehydration process [34]. First, one molecule H_2O is lost, forming

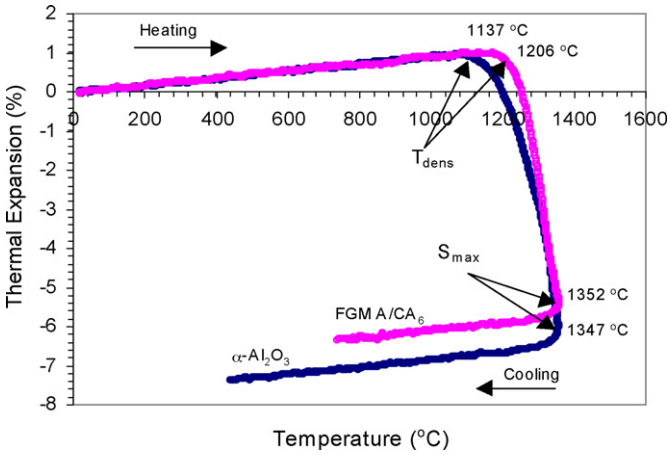

Fig. 2. Thermal expansion and shrinkage behaviour for the functionally graded A/CA_6 composites and alumina for the temperature range 20–1500 °C. T_{dens} indicates the temperature at which densification commences and S_{max} indicates the maximum shrinkage.

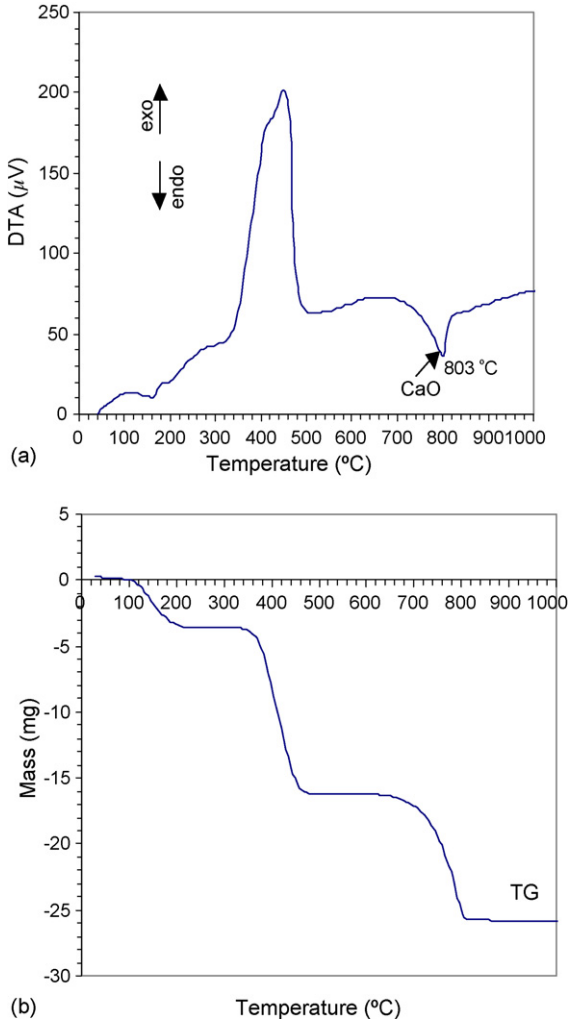

Fig. 3. Thermal analysis for calcium acetate in the temperature range 20–1000 °C: (a) DTA and (b) TGA.

$Ca(CH_3COO)_2{\cdot}H_2O$, and its subsequent formation of semihydrate $Ca(CH_3COO)_2{\cdot}0.5H_2O$ that becomes anhydrous at 180–220 °C given by:

$$Ca(CH_3COO)_2{\cdot}H_2O + H_2O \rightarrow Ca(CH_3COO)_2{\cdot}2H_2O \quad (3)$$

$$Ca(CH_3COO)_2{\cdot}2H_2O \rightarrow Ca(CH_3COO)_2{\cdot}H_2O + H_2O \quad (4)$$

$$Ca(CH_3COO)_2{\cdot}H_2O \rightarrow Ca(CH_3COO)_2{\cdot}0.5H_2O + 0.5H_2O \quad (5)$$

$$Ca(CH_3COO)_2{\cdot}0.5H_2O \rightarrow Ca(CH_3COO)_2 + 0.5H_2O \quad (6)$$

By further heating calcium acetate decomposes at temperatures between 340 and 480 °C with releasing volatiles, acetone in an oxidising and forming $CaCO_3$ given by:

$$Ca(CH_3COO)_2 \rightarrow CaCO_3 + CH_3COCH_3 \quad (7)$$

The acetone, CH_3COCH_3 further decomposes at high temperatures to allene, $CH_2{=}C{=}CH_2$ and this compound can be burnt with oxygen [35]. The endothermic peak at 803 °C corresponds to the decomposition of the residual carbonate $CaCO_3$ to form calcium oxide CaO and carbon dioxide CO_2 as follows:

$$CaCO_3 \rightarrow CaO + CO_2 \quad (8)$$

Fig. 4 shows the simultaneous DTA and TGA results for the graded alumina/CA_6 sample as recorded in the temperature range 20–1500 °C. An exothermic peak appears at ~435 °C can be related to the removal of absorbed water, residual hydroxyl groups, and organic materials and decomposition of calcium acetate. The endothermic peak at ~763 °C which can be associated with the substantial weight losses on the TGA curve (Fig. 3b), indicates the decomposition of calcium carbonate to form calcium oxide. Interestingly, there was no endothermic or exothermic peaks observed at ~1350 °C due to the formation of CA_6 phase. This suggests that the rate formations for the calcium aluminates (CA, CA_2, and CA_6) phases are very sluggish and the growth of the calcium aluminates is diffusion-controlled and strongly time-dependent.

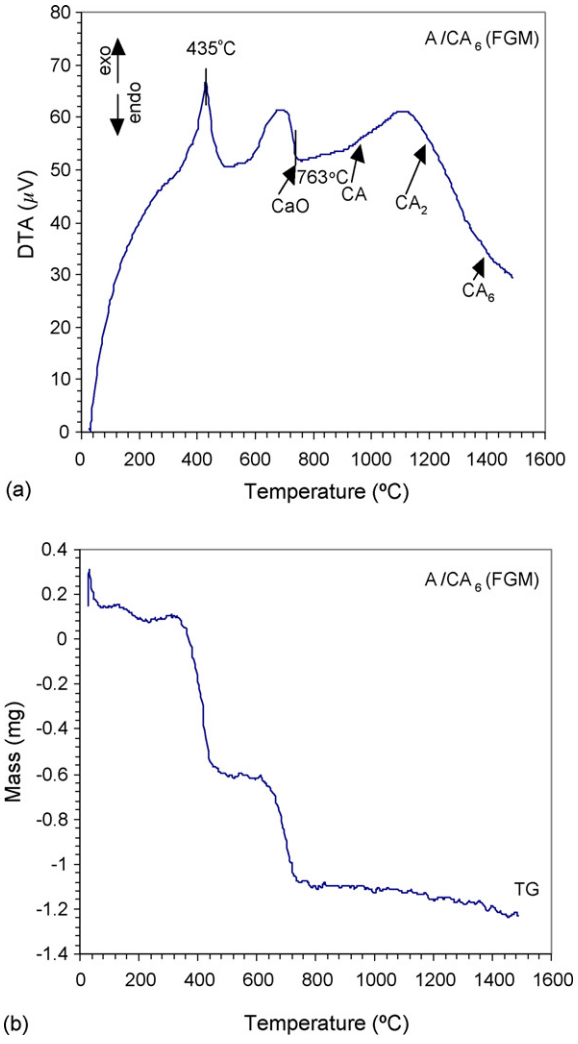

Fig. 4. Thermal analysis for the graded alumina/CA_6 sample in the temperature range 20–1000 °C; (a) DTA and (b) TGA.

3.4. Mechanical properties

The Vickers hardness measurement as a function of depth for the FGM sample from the graded alumina/CA_6 layer to the homogeneous alumina layer was performed on the polished surface. Indentation was made at the distances corresponding to ~1.0, 2.9, 4.2, 5.9, 7.6, 9.9, 12.3, 15.1, 17.0, and 18.0 mm from the graded layer. Fig. 5 shows the variation of Vickers hardness as a function of distance for the graded sample, i.e. from the graded layer to the non-graded Al_2O_3 region, as well as the average hardness for the control sample. It is evident the hardness increased markedly from the graded region to the non-graded region and then leveled-out. At ~1.0 mm distance, the hardness of material was only 10.6 GPa, then markedly increased to 17.2 GPa at ~9.9 mm distance, followed by a steady increase thereafter. This display of graded variations in hardness is expected since the concentration of relatively soft CA_6 decreases with distance as confirmed by our synchrotron radiation and X-ray diffraction results previously reported

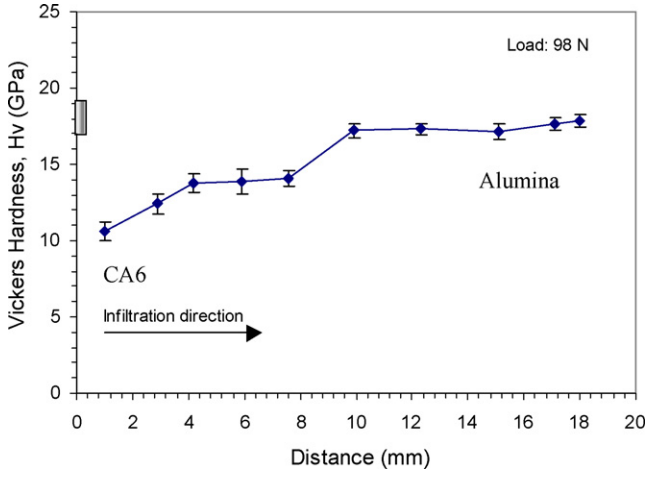

Fig. 5. Variation of Vickers hardness as a function of distance for the graded alumina/CA_6 sample tested at a load of 98 N. The shaded box at the left represents the average Vickers hardness for the alumina control sample. Error bars indicate two estimated standard deviations (2σ).

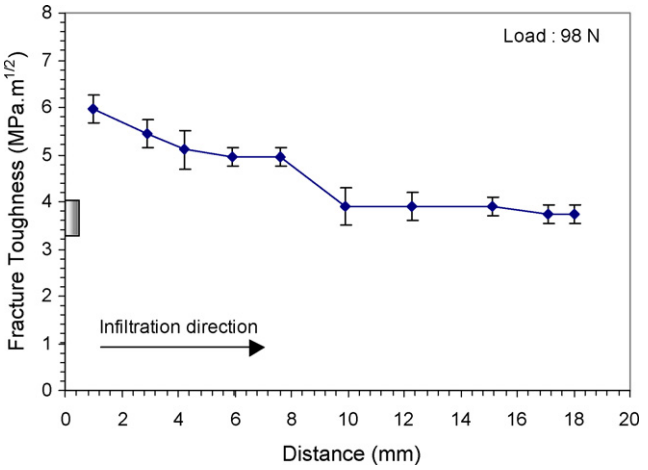

Fig. 6. Variation of fracture toughness as a function of distance for the graded sample tested at a load of 98 N. The shaded box at the left represent the average fracture toughness for the alumina control sample. Error bars indicate two estimated standard deviations (2σ).

[36,37]. The average hardness of 17.5 GPa in non-graded region is only slightly lower than that of 17.8 GPa measured for the alumina control sample.

Fig. 6 shows the variations of fracture toughness as a function of distance for the graded sample, i.e. from the graded region to the non-graded alumina region. The average fracture toughness for the alumina control sample is also shown. It is evident that the fracture toughness decreased gradually with increasing distance in the graded region and leveled-out in the non-grade region. At ~1.0 mm distance, the fracture toughness of material is 6.0 MPa $m^{1/2}$, then decreased to 3.9 MPa $m^{1/2}$ at ~9.9 mm distance and leveled-out thereafter. Again, this display of graded variations in fracture toughness is expected since the concentration of relatively soft CA_6 decreases with distance [36,37]. The display of a higher fracture toughness in the graded region than the non-graded alumina region can be attributed to the presence of elongated CA_6 grains which has imparted crack-energy dissipation through crack deflection and crack-bridging. These crack–tip interactions with the CA_6 platelets are evident in the back-scattered electron image shown in Fig. 7.

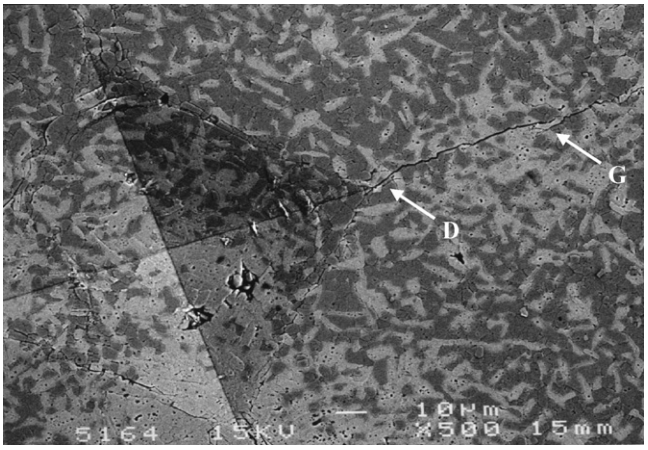

Fig. 7. Back-scattered electron micrograph of a graded alumina/CA_6 sample with a Vickers indent showing crack deflection (labeled as 'D') and crack-bridging (labeled as 'G').

4. Conclusion

The presence of CA_6 phase in Al_2O_3 matrix has a significant effect on the physical, thermal, and mechanical properties of the graded alumina/CA_6 composite. The presence of CA_6 has hindered slightly the process of sintering and densification in alumina matrix. The graded composites exhibited a lower hardness in the graded-region (A/CA_6) than the non-graded alumina region which can be attributed to the presence of a large amount of relatively soft CA_6 in the former. Similarly, the fracture toughness decreased gradually with increasing distance in the graded region and leveled-out in the non-graded region. The improved fracture toughness in the graded region can be attributed to the display of energy dissipative processes such as crack deflection and crack-bridging by the CA_6 platelets.

Acknowledgements

We are grateful to AINSE for providing funding (98/010 and 99/029) to support this work. D. Asmi is grateful to the World Bank through the DUE Project University of Lampung, Indonesia for granting a research scholarship.

References

[1] G.C. Wei, P.F. Becher, Development of SiC-whisker-reinforced ceramic, Am. Ceram. Soc. Bull. 64 (1985) 298–304.
[2] P.F. Becher, C.H. Hsueh, P. Angelini, T.N. Tiegs, Toughening behaviour in whisker-reinforced ceramic matrix composites, J. Am. Ceram. Soc. 71 (1998) 1050–1061.
[3] H. Sakai, K. Matsuhiro, Y. Furuse, Mechanical properties of SiC platelet reinforced ceramic composites, in: D. Sacks (Ed.), Ceramic Transactions, vol. 19, 1991, pp. 765–771.
[4] D.E. Garcia, R. Janssen, N.E. Claussen, Microstructure development in in-situ reinforced reaction-bonded alumina niobate-based composites, J. Am. Ceram. Soc. 79 (1996) 2266–2270.
[5] T. Carisey, W.A. Laugier, D.G. Brandon, Control of texture in Al_2O_3 by gel-casting, J. Eur. Ceram. Soc. 15 (1995) 1–8.
[6] M. Belmonte, R. Moreno, J.S. Moya, P. Miranzo, Obtention of highly dispersed platelet-reinforced Al_2O_3 composites, J. Mater. Sci. 29 (1994) 179–183.
[7] T. Carisey, I. Levin, D.G. Brandon, Microstructure and mechanical properties of textured Al_2O_3, J. Eur. Ceram. Soc. 15 (1995) 283–289.
[8] P.F. Becher, G.S. Painter, E.Y. Sun, C.H. Hsueh, M.J. Lance, The importance of amorphous intergranular films in self-reinforced Si_3N_4 ceramics, Acta Mater. 48 (2000) 4493–4499.
[9] P.F. Becher, E.Y. Sun, K.P. Plucknett, K.B. Alexander, C.H. Hsueh, H.T. Lin, S.B. Waters, C.G. Westmoreland, E.S. Kang, K. Hirao, M. Brito, Microstructural design of Si_3N_4 with improved fracture toughness: I, effects of grain shape and size, J. Am. Ceram. Soc. 81 (1998) 2821–2830.
[10] K. Hirao, H. Imamura, K. Watari, M.E. Brito, M. Toriyama, S. Kanzaki, Seeded Si_3N_4: microstructure and performance, Key Eng. Mater. 161–163 (1999) 469–474.
[11] C.S. Lee, Y.W. Kim, D.H. Cho, H.B. Lee, H.J. Lim, Microstructure and mechanical properties of self-reinforced α-SiC, Ceram. Int. 24 (1998) 489–495.
[12] N.P. Padture, In-situ toughened silicon carbide, J. Am. Ceram. Soc. 77 (1994) 519–523.

[13] L. An, H.M. Chan, K.K. Soni, Control of calcium hexaluminate grain morphology in in-situ toughened ceramic composites, J. Mater. Sci. 31 (1996) 3223–32229.
[14] D. Asmi, I.M. Low, Processing of an in-situ layered and graded calcium hexaluminate/alumina composite: I, physical characteristics, J. Eur. Ceram. Soc. 18 (1998) 2019–2025.
[15] D. Asmi, I.M. Low, Physical and mechanical characteristics of in-situ Al_2O_3/CA_6 composites, J. Mater. Sci. Lett. 17 (1998) 1735–1738.
[16] D. Asmi, I.M. Low, S. Kennedy, R.A. Day, Characteristics of a layered and graded alumina/calcium-hexaluminate composite, Mater. Lett. 40 (1999) 96–102.
[17] P.L. Chen, I.W. Chen, In-situ alumina/aluminate platelet composites, J. Am. Ceram. Soc. 75 (1992) 2610–2613.
[18] M. Yasuoka, K. Hirao, M.E. Brito, S. Kanzaki, High strength and high toughness ceramics in the $Al_2O_3/LaAl_{11}O_{18}$ systems, J. Am. Ceram. Soc. 78 (1995) 1853–1858.
[19] S. Maschio, G. Pezzotti, Microstructural development and mechanical properties of alumina-hexaluminate composites as-sintered and after aging in aqueous and physiological solution, J. Ceram. Soc. Jpn. 107 (1999) 270–274.
[20] K. Vishista, F.D. Gnanam, H. Awaji, Sol-gel synthesis and characterization of alumina-calcium hexaaluminate composites, J. Am. Ceram. Soc. 88 (2005) 1175–1179.
[21] L. An, H.M. Chan, R-curve behaviour of in-situ toughened $Al_2O_3/CaAl_{12}O_{19}$ ceramic composites, J. Am. Ceram. Soc. 79 (1996) 3142–3148.
[22] L. An, H.C. Ha, H.M. Chan, High-strength alumina/alumina-calcium hexaluminate layer composites, J. Am. Ceram. Soc. 81 (1998) 3321–3324.
[23] L. An, H.M. Chan, N.P. Padture, B.R. Lawn, Damage-resistant alumina-based layer composites, J. Mater. Res. 11 (1996) 204–210.
[24] S.J. Glass, D.J. Green, Surface modification of ceramics by partial infiltration, Adv. Ceram. Mater. 2 (1987) 129–131.
[25] B.R. Marple, D.J. Green, Mullite/alumina particulate composites by infiltration processing: II, infiltration and characterization, J. Am. Ceram. Soc. 73 (1990) 3611–3616.
[26] I.M. Low, R. Skala, R. Richards, D.S. Perera, Synthesis and properties of novel mullite/zirconia-toughened alumina composites, J. Mater. Sci. Lett. 12 (1993) 1585–1587.
[27] S. Pratapa, I.M. Low, B. O'Connor, Infiltration-processed functionally-graded AT/alumina-zirconia composites: I, microstructural characterisation and physical properties, J. Mater. Sci. 33 (1998) 3037–3045.
[28] S. Pratapa, I.M. Low, Infiltration-processed functionally-graded AT/alumina-zirconia composites: II, mechanical properties, J. Mater. Sci. 33 (1998) 3047–3053.
[29] I.M. Low, R. Skala, D. Zhou, Synthesis and properties of gel-derived functionally graded ceramics, in: F.D. Guanam (Ed.), Proceedings of the International Workshop on Sol–Gel Processing of Advanced Ceramics, Oxford and IBH Publisher, New Delhi, 1996, pp. 143–158.
[30] I.M. Low, Processing of an in-situ layered and graded aluminium-titanate/alumina composites, Mater. Res. Bull. 33 (1998) 1475–1481.
[31] Australian Standard 1774.5, Refractories and refractory material—physical test methods, in: Method 5: The Determination of Density, Porosity and Water Absorption, Standards Australia, Sydney, 1989, p. 14.
[32] E. Criado, P. Pena, A. Caballero, Influence of processing method on microstructural and mechanical properties of calcium hexaluminate compacts, Sci. Ceram. 12 (1988) 193–198.
[33] K. Kato, H. Saalfeld, Verfeinerung der kristallstruktur von $CaO{\cdot}6Al_2O_3$, Neues Jahrbuch fuer Mineralogie 109 (1968) 192–200.
[34] V.T. Orlova, A.A. Frolov, O.N. Evstaff'eva, Interaction in the system $Mg(CH_3COO)_2$–$Ca(CH_3COO)_2$–H_2O, Russ. J. Inorg. Chem. 38 (1993) 1914–1917.
[35] J. Adánez, L.F. de Diego, F. Gracía-Labiano, Calcination of calcium acetate and calcium magnesium acetate: effect of the reacting atmosphere, Fuel 78 (1999) 583–592.
[36] D. Asmi, I.M. Low, B.H. O'Connor, C. Buckley, Phase compositions and depth-profiling of calcium-aluminates in a functionally-graded Al_2O_3/CA_6 composite, J. Mater. Proc. Tech. 118 (2001) 219–224.
[37] M. Singh, D. Asmi, I.M. Low, Depth profiling of a functionally graded alumina/calcium-hexaluminate composite using grazing incidence synchrotron-radiation diffraction, J. Eur. Ceram. Soc. 22 (2002) 2877–2882.